

Durham Research Online

Deposited in DRO:

03 April 2018

Version of attached file:

Accepted Version

Peer-review status of attached file:

Peer-reviewed

Citation for published item:

Petrick, B. and McClymont, E.L. and Littler, K. and Rosell-Melé, A. and Clarkson, M.O. and Maslin, M. and Röhl, U. and Shevenell, A.E. and Pancost, R.D. (2018) 'Oceanographic and climatic evolution of the southeastern subtropical Atlantic over the last 3.5 Ma.', *Earth and planetary science letters*, 492 . pp. 12-21.

Further information on publisher's website:

<https://doi.org/10.1016/j.epsl.2018.03.054>

Publisher's copyright statement:

© 2018 This manuscript version is made available under the CC-BY-NC-ND 4.0 license
<http://creativecommons.org/licenses/by-nc-nd/4.0/>

Additional information:

Use policy

The full-text may be used and/or reproduced, and given to third parties in any format or medium, without prior permission or charge, for personal research or study, educational, or not-for-profit purposes provided that:

- a full bibliographic reference is made to the original source
- a [link](#) is made to the metadata record in DRO
- the full-text is not changed in any way

The full-text must not be sold in any format or medium without the formal permission of the copyright holders.

Please consult the [full DRO policy](#) for further details.

Oceanographic and climatic evolution of the southeastern subtropical Atlantic over the last 3.5 Ma

Benjamin Petrick^{1,2}; Erin L. McClymont³; Kate Littler⁴; Antoni Rosell-Melé^{5,6}; Matthew O. Clarkson⁷; Mark Maslin⁸, Ursula Röhl⁹; Amelia E. Shevenell^{8,10}; Richard D Pancost¹¹

1. Max Planck Institute of Chemistry, Climate Geochemistry Department, Hahn-Meitner-Weg 1,

55128 Mainz Germany

2. Department of Geography, Newcastle University,

3. Department of Geography, Durham University, South Road, Durham, DH1 3LE, U.K.

4. Camborne School of Mines & Environment and Sustainability Institute University of Exeter

5. Institute of Environmental Science and Technology, Autonomous University of Barcelona, Campus

de la UAB 08193 Bellaterra (Cerdanyola del Vallès), Barcelona, Spain

6. Institució Catalana de Recerca i Estudis Avançats, 08010 Barcelona, Catalonia, Spain.

7. Institute of Geochemistry and Petrology, Department of Earth Sciences, ETH, 8092, Zurich,

Switzerland

8. Department of Geography University College London, Pearson Building, Gower Street, London,

WC1E 6BT

9. MARUM – Center for Marine Environmental Sciences, University of Bremen, Leobener Str. 8,

28359 Bremen, Germany

10. College of Marine Science, University of South Florida, St. Petersburg, FL 33701, USA

11. University of Bristol School of Chemistry, Cantock's Close, BS8 1TS, Bristol UK

Abstract

The southeast Atlantic Ocean is dominated by two major oceanic systems: the Benguela

Upwelling System, one of the world's most productive coastal upwelling cells and the Agulhas

Leakage, which is important for transferring warm salty water from the Indian Ocean to the Atlantic

Ocean. Here, we present a multi-proxy record of marine sediments from ODP Site 1087. We reconstruct sea surface temperatures (U_{37}^K and TEX_{86} indices), marine primary productivity (total chlorin and alkenone mass accumulation rates), and terrestrial inputs derived from southern Africa (Ti/Al and Ca/Ti via XRF scanning) to understand the evolution of the Southeast Atlantic Ocean since the late Pliocene. In the late Pliocene and early Pleistocene, ODP Site 1087 was situated within the Benguela Upwelling System, which was displaced southwards relative to present. We recognize a series of events in the proxy records at 3.3, 3.0, 2.2, 1.5, 0.9 and 0.6 Ma, which are interpreted to reflect a combination of changes in the location of major global wind and oceanic systems and local variations in the strength and/or position of the winds, which influence nutrient availability. Although there is a temporary SST cooling observed around the initiation of Northern Hemisphere glaciation (iNHG), proxy records from ODP Site 1087 show no clear climatic transition around 2.7 Ma but instead most of the changes occur before this time. This observation is significant because it has been previously suggested that there should be a change in the location and/or strength of upwelling associated with this climate transition. Rather, the main shifts at ODP Site 1087 occur at ca. 0.9 Ma and 0.6 Ma, associated with the early mid-Pleistocene transition (EMPT), with a clear loss of the previous upwelling-dominated regime. This observation raises the possibility that reorganisation of southeast Atlantic Ocean circulation towards modern conditions was tightly linked to the EMPT, but not to earlier climate transitions.

1.1 Introduction

Over the last 3.5 Ma, Earth's climate transitioned from warmer climates of the Pliocene to cooler Pleistocene climates (Haug et al., 2005; McClymont et al., 2013). Two of the biggest climate transitions were the intensification of Northern Hemisphere glaciation (iNHG; 3.0 and 1.5 Ma), when Northern Hemisphere ice sheets expanded and the oceans cooled (Haug et al., 2005), and the early mid-Pleistocene transition (EMPT; 1.2 and 0.6 Ma), when glacial-interglacial cycles shifted to a quasi-

100ka period (Chalk et al., 2017; Maslin and Brierley, 2015; McClymont et al., 2013). Shifts in the location and intensity of the major ocean upwelling cells are thought to play an important role in global climate during the Plio-Pleistocene (Lawrence et al., 2013; März et al., 2013). For example, the equatorward migration of the major wind cells between 3.3 and 1.0 Ma resulted in a concomitant shift of the subtropical and polar upwelling zones and increased global carbonate production, affecting the global atmosphere-ocean CO₂ exchange (Lawrence et al., 2013; Martínez-García et al., 2011). Additionally, models show that cooler sea surface temperatures (SSTs) in upwelling zones can affect mean global atmospheric temperatures, as upwelling cells supply cooler deeper waters to the surface ocean (Barreiro et al., 2005).

Debate exists about the precise timing of upwelling shifts during the Plio-Pleistocene and whether the changes in location and focus of the different upwelling systems reflect local, rather than global, factors (Dekens et al., 2007; Lawrence et al., 2013; Rosell-Melé et al., 2014). Lawrence et al. (2013) proposed that between 3.3 and 2.5 Ma, the build-up of ice sheets in the Northern Hemisphere caused the westerlies to shift equatorward and the Hadley Cells to contract, shifting the location of the trade winds. These authors propose that the shift in the wind fields resulted in cooling and increased productivity in major North and South Atlantic Ocean upwelling cells. Others have suggested, based on SST cooling around 3.3 Ma (Dekens et al., 2007), that upwelling cells were invigorated before the intensification of glacial stages at 2.7 Ma (MIS 96-100) (Haug et al., 2005). Later upwelling intensification in the Benguela System around 2 Ma has been inferred from SST cooling and increased productivity (Etourneau et al., 2010, 2009). Thus, it remains unclear whether changes in upwelling activity across the Plio-Pleistocene transition were influenced by global climate transitions or occurred independently.

ODP Site 1087 (31°28'S, 15°19'E; 1374 m water depth) is located near the southern cell of the modern Benguela Upwelling System (Figure 1). Foraminiferal assemblages, SST reconstructions, and marine organic matter inputs indicate that ODP Site 1087 was influenced by the Benguela

Upwelling System during the Pliocene (3.5–3.0 Ma; Petrick et al., 2015a). However, during the mid to late Pleistocene (0–0.6 Ma), foraminiferal assemblage, SST, and salinity records indicate that the site was primarily influenced by Indian Ocean waters via the Agulhas Leakage, with evidence of upwelling limited to a few glacial periods (Caley et al., 2014, 2012; McClymont et al., 2005; Petrick et al., 2015b). What remains unclear is the nature and timing of the transition from an upwelling-dominated to a leakage-dominated regime, and whether this shift occurred as part of the iNHG or the EMPT. The timing of this transition may have important climatic implications, as intensification of Agulhas leakage enhances heat and salt transfer into the Southeast Atlantic Ocean, which may influence the strength of the AMOC (Biaosoch et al., 2008). The continuous Plio-Pleistocene sediment sequence from ODP Site 1087 provides an ideal archive from which to reconstruct the evolution of the southern Benguela Upwelling and Agulhas Leakage Systems over the Plio-Pleistocene.

1.2 Oceanographic Setting and paleoclimate history

The Benguela Upwelling System is a key oceanographic upwelling region that developed around the mid-Miocene (Diester-Haass, 1988). The Benguela Upwelling is one of the few major temperate upwelling sites in the world. It is an area that releases CO² and is important for biological cycling in the ocean (Compton et al., 2009; West et al., 2004). Therefore, understating the history of the System under different climate regimes is important for understanding the effects and impacts of climate change. It has been proposed that the main focus of the Benguela Upwelling System has migrated northward from the southern Benguela region to its current location since the mid-Pliocene (Christensen and Giraudeau, 2002; Petrick et al., 2015a; Rosell-Melé et al., 2014). Changes in temperature and productivity have been well documented in the northern (ODP Sites 1082 and 1081; Figure 1) and central Benguela upwelling cells (ODP Site 1084) over the last 3.5 Ma (Etourneau et al., 2009; Marlow et al., 2000; Rosell-Melé et al., 2014). Initial cooling began gradually in the northern and central cells around 3.5 Ma, with a 0–1°C gradient from the northern to central

upwelling cells (Rosell-Melé et al., 2014). Around 3.0 Ma, there was an increase in diatom production, marking the Matuyama Diatom Maximum (MDM), in the northern and central Benguela regions (3.0–2.5 Ma) (Robinson and Meyers, 2002). Around 1.5 Ma, there was major cooling at all three sites and the development of a 3–4°C gradient between the northern and central cells (Rosell-Melé et al., 2014). Regional primary productivity was stable until 2.4 Ma, when it increased in the central cells (Rosell-Melé et al., 2014); productivity increased in the northern cells at 0.6 Ma (Rosell-Melé et al., 2014). Constriction and northward movement of the Hadley cells since the Pliocene is hypothesized to have shifted the focus of upwelling equatorward (Etourneau et al., 2010; Rosell-Melé et al., 2014). More recently, models indicate that tectonic mountain-building in West Africa may have influenced the position and intensity of the trade winds, resulting in the onset and northward migration of upwelling since the mid-Miocene (Jung et al., 2014).

Presently, sea surface conditions at ODP Site 1087 are influenced by the Agulhas Leakage (Figure 1) (Gordon et al., 1987; Gordon and Haxby, 1990), which transfers rings of warm and salty water from the Indian Ocean to the Atlantic Ocean. This is the primary way that surface water is transferred from the Indian Ocean to the Atlantic Ocean. These rings are then advected northwards and ultimately incorporated into the Atlantic Meridional Overturning Circulation (AMOC) (Hall and Lutjeharms, 2011). Through its impact on salt transfer to the North Atlantic, the intensity of Agulhas Leakage has been shown to influence the strength of the AMOC over centennial to millennial scale times (Björnsdóttir et al., 2008; Knorr and Lohmann, 2003). In climate models, increases in the Agulhas Leakage are able to restart the thermohaline circulation after a period of shutdown, for example in response inputs of fresh waters to the North Atlantic; (Knorr and Lohmann, 2003). Increased Agulhas Leakage has also been shown to be a prominent feature of deglaciations over the last 1200 kyr (Beal et al., 2011) and may have prevented an early return to glacial conditions, such as during the Younger Dryas, through increasing input of high salinity waters to the source of the Atlantic thermohaline circulation (Dyez et al., 2014; Marino et al., 2013; Scussolini et al., 2015). Furthermore, other studies have shown that this salt leakage seems to have existed since at least

500ka (Petrick et al., 2015)

Today, ODP 1087 does not receive much terrestrial input. The modern day site is on the edge of the Namibian Dust Plume (Kienast et al., 2016; Mahowald et al., 2014). Therefore the amount of dust reaching the site is limited. Additionally, the Orange River provides a minor source of riverine input. While the majority of the input from the Orange River occurs far north of the site, some finer particles are incorporated into the turbulent Cape Basin Area (Bluck et al., 2007; Boebel et al., 2003; Compton and Maake, 2007). These then are transported throughout the Cape Basin (Boebel et al., 2003). However, overall the amount of terrestrial material is low compared to other sites in the region.

ODP Site 1087 preserves evidence of both Agulhas Leakage and Benguela Upwelling in the same core, so it is ideal for understanding the relationship between these two oceanic systems. In order to track shifts in upwelling strength over the last 3.5 Ma, we applied a multiproxy approach to sediments from ODP Site 1087 (Figure 1). Two biomarker temperature proxies, the U_{37}^K and TEX_{86} indices (Müller et al., 1998; Schouten et al., 2002), were used to reconstruct SSTs, which are sensitive to upwelling strength. Additionally, concentrations of chlorins and alkenones were determined to assess primary productivity and coccolithophore productivity, respectively (Harris et al., 1996). Ca/Ti ratios from XRF scanning were used as a proxy of carbonate deposition/preservation at the site, which may relate to changes in productivity. Terrestrial inputs were assessed using Ti/Al counts, which have been shown for the SE Atlantic to track dust over riverine input (Govin et al., 2012). For more information about the Interpretation and complications of the proxy signals, see the supplemental data.

The U_{37}^K -derived SSTs and alkenone mass accumulation rate (MAR) data for the last 1.5 Ma are published (McClymont et al., 2005; Petrick et al., 2015a). However, the new data we present allow a better understanding of: 1) Changes in the vertical temperature structure of the upper water column (U_{37}^K - TEX_{86}), which gives an indication of upwelling strength, because research shows that

in Benguela sourced water SST reconstructions are lower in TEX_{86} than U_{37}^K . By comparing periods where the two proxies record different temperature to those where the SSTs are the same, we can track the presence of upwelling sourced water; 2) Changes in terrestrial inputs (Ti/Al) and potential wind-forcing of any upwelling changes; and 3) Associated changes in marine productivity (alkenone and chlorin MAR). These new data are placed in a regional context through comparison to similar datasets from the northern and central Benguela Upwelling System (ODP Sites 1081, 1082, and 1084; Fig. 1).

2. Methods

ODP Site 1087 is located in the SE Atlantic Ocean (Shipboard Scientific Party, 1998) (Figure 1). All of the sediments analysed in this study are from the shipboard-defined lithologic "Unit I", which is described as a moderately bioturbated olive to olive-grey foraminifera-nannofossil ooze, with 50-100 cm thick nannofossil oozes in the upper 45 m (Shipboard Scientific Party, 1998). The age model between 0-1.5 Ma and 3.0-3.5 Ma and sampling strategy are based on foraminifera oxygen isotope stratigraphies tuned to the LR04 $\delta^{18}\text{O}$ stack (McClymont et al., 2005; Petrick et al., 2015a, 2015b). We assume linear sedimentation rates between the shipboard nanofossil model tie-points between 1.5-3.0 Ma (Shipboard Scientific Party, 1998). The average sampling resolution is 5 cm, which translates to a temporal resolution of 3-kyr in the Pliocene and mid- to late-Pleistocene, and 10-kyr in the early Pleistocene.

2.1 Biomarker analysis

The biomarkers (alkenones, chlorins, and glycerol dialkyl glycerol tetraethers (GDGTs)) were extracted from homogenised, freeze-dried sediment using a CEM microwave system with 12 ml of DCM:MeOH (3:1, v/v). Internal standards were added for quantification (5 α -cholestane, dotriacontane and tetracontane). The microwave temperature programme heats samples to 70°C over a 5 minute temperature ramp, holds temperatures at 70°C for 5 minutes, and then cools over 30 minutes (Kornilova and Rosell-Mele, 2003). The supernatant was decanted into vials and dried

under a nitrogen stream. An aliquot was taken for chlorin concentration and TEX₈₆ analyses and the remainder was derivatised using N,O- Bis(trimethylsilyl)trifluoroacetamide with trimethylchlorosilane at 70 °C for 1 hour before alkenone analysis.

Alkenones were analysed using a gas chromatograph fitted with a flame-ionisation detector (GC-FID) and a 30 m HP1-MS capillary column. The injector temperature was held at 300°C and the detector at 310°C. The oven program is as follows: after injection, hold at 60°C for 1 min, increase to 120°C at 20°C m⁻¹, to 310°C at 6°C m⁻¹, and hold at 310°C for 30 min. The alkenone abundances were converted to MAR using linear sedimentation rates and the shipboard dry bulk density measurements (Shipboard Scientific Party, 1998). The U₃₇^K' was calculated using the relative abundances of the C_{37:3} and C_{37:2} alkenones (Prahl and Wakeham, 1987), and converted to SSTs using the Müller et al. (1998) core-top calibration. The error associated with the analytical measurement is ±0.5°C, while the calibration error equates to ±1.0°C (Müller et al., 1998).

A subset of samples was selected for TEX₈₆ analysis, guided by our U₃₇^K' results, with the aim of ensuring a broad spectrum of both warm and cold periods was represented. The GDGT fraction was re-dissolved in 200 µl of hexane:n-propanol (98.5:1.5, v/v) and an internal standard was added. The sample and standard was filtered through a 0.5 µm PTFE filter. The filtered samples were analysed by High-Performance Liquid Chromatography Mass Spectrometry (HPLC-MS), using a Dionex P680 HPLC coupled to a Thermo Finnigan TSQ Quantum Discovery Max quadrupole mass spectrometer at the University of Barcelona Automatica, with an atmospheric pressure chemical ionization (APCI) interface set in positive mode. The GDGTs were eluted through a Tracer Excel CN column (Teknokroma) with a length of 20 cm, a diameter of 0.4 cm and a particle size of 3 µm. There was a guard column on the other end of the set-up. The mobile phase was initially hexane:n-propanol (98.5:1.5) at a flow of 0.6 mL min⁻¹. The proportion of n-propanol was kept constant at 1.5% for 4 minutes, increased gradually to 5% during 11 minutes, increased to 10% for 1 minute, held for 4 minutes, decreased back to 1.5% during 1 minute, and held at these conditions for 9

minutes. The parameters of the APCI interface were set as follows to generate positive ion spectra: corona discharge 3 μ A, vaporizer temperature 400 $^{\circ}$ C, sheath gas pressure 49 mTorr, auxiliary gas (N₂) pressure 5 mTorr, and capillary temperature 200 $^{\circ}$ C. A subset of samples was analysed using the HPLC system at University College London (UCL). The error associated with the analytical measurement is $\pm 1.0^{\circ}$ C, while the calibration error (BAYSPAR; Tierney and Tingley, 2014) varies according to geographic location, but on average for this record equates to $\pm 7.0^{\circ}$ C at 95% confidence.

Chlorins were analysed using an HPLC system coupled to a photo-diode array spectrophotometer. Solvent extracts were dissolved in acetone and injected three times. The PDA scanned across 350 – 800 nm and absorbance at the wavelengths 410 and 665 nm was quantified. Sample means of the triplicate measurements are reported here. Analytical variability was monitored using repeat measurements of a standard and was determined at 0.07 absorbance units (abs). For all samples, the absorbance at 410 nm or 665 nm was divided by the total dry weight of the sample to calculate absorbance/g and then converted to mass accumulation rate (MAR) using the linear sedimentation rates and the shipboard dry bulk density measurements (Zachos et al., 2004).

2.2 XRF analysis

Elemental data was collected using an XRF Core Scanner II (AVAATECH Serial No. 2) at the MARUM, University of Bremen. The reported data here have been acquired by a Canberra X-PIPS Silicon Drift Detector (SDD; Model SXD 15C-150-500) with 150eV X-ray resolution, the Canberra Digital Spectrum Analyser DAS 1000, and an Oxford Instruments 50W XTF5011 X-Ray tube with rhodium (Rh) target material. Elements (Fe, Ca, Ti) were collected at a resolution of 2-cm down-core, over a 2 cm² area with down-core slit size of 10 mm, using generator settings of 10 kV, a current of 0.15 mA, and a sampling time of 20 seconds directly at the split core surface of the archive half. The split core surface was covered with a 4-micron thin SPEXCerti Prep Ultralene1 foil to avoid

contamination of the XRF measurement unit and desiccation of the sediment. Raw data spectra were processed by the analysis of X-ray spectra by the Iterative Least Square software (WIN AXIL) package from Canberra Eurisys. Due to previous oversampling, it was impossible to scan the upper four sections of the core. Additionally, because of the time between the core being taken and the XRF scanning, it was impossible to normalize the XRF scanning data to the initial shipboard data.

3. Results

3.1 Sea surface temperature trends

Two separate biomarker indices were used to calculate SSTs: higher resolution data using the U_{37}^K proxy (from alkenones), and lower resolution data using the TEX_{86} proxy (from GDGTs). For more information about the calibrations used, see supplemental data. Over the last 3.5 Ma, U_{37}^K -derived SST values at ODP Site 1087 range between 12 and 24°C (Figures 2 and 3), with an average of around 18°C. Overall, the SST trends can be summarised as: stable SSTs between 3.5 and 1.7 Ma, 3° C cooling between 1.7 and 0.9 Ma, and 2° C warming SSTs from 0.9 Ma to present (Figures 2 and 3). The coldest SSTs of 12°C occurred around 0.5 Ma (Marine Isotope Stage (MIS) 13). The highest SST variability (~10°C) across glacial-interglacial timescales occurs after 0.9 Ma.

The lower resolution TEX_{86} -derived SSTs range from 10 to 24°C over the last 3.5 Ma, with an average of ~16 °C (Figure 2). The SSTs were relatively stable before ~0.9 Ma, after which there is increased variability in the data and evidence for 2° C warming towards the present. Before 0.9 Ma, the TEX_{86} -derived SSTs are cooler than coeval U_{37}^K -derived SSTs by up to 10°C. After 0.9 Ma, TEX_{86} -derived SSTs are either similar to, or warmer than, the U_{37}^K -derived SSTs. The difference between the two temperature proxies indicates that the U_{37}^K temperatures are only cooler after 0.6 Ma (Figure 2).

3.2 Productivity proxies

Three proxies were used to track changes in the primary productivity of the site: 1) chlorin MAR; 2) alkenone mass accumulation rates (MAR); and 3) Ca/Ti ratios generated from XRF scanning. Chlorin MARs range between 0.001 and 1.0 g² abs cm⁻² kyr⁻¹ (Figure 3). Between 1.7 and 0.5 Ma, chlorin MARs are elevated, which contrasts with low values (<0.05 abs cm⁻² kyr⁻¹) between 3.0–1.7 Ma. A return to low chlorin MARs for the last 0.4 Ma is recorded after a final high peak in chlorins during MIS 10. Alkenone MAR ranges between 1 and 12 µg cm⁻² kyr⁻¹, with an overall zone of low amplitude oscillations between 3.0 and 2.5 Ma (Figure 3). After 0.9 Ma, the highest values occur in MISs 14, 12, 10, and 8. Ca/Ti values range between 100 and 1800 (Figure 4). The lowest values are around 3.1 Ma; with a slight increase around 3.0 Ma, followed by stable Ca/Ti ratios. Ca/Ti then increases towards the modern day, starting around 1.6 Ma, with the highest values around 0.4 Ma, although there are no glacial-interglacial trends in the data.

3.3 Terrestrial proxy

Ti counts range from 1000 to 8000 counts at ODP Site 1087 (Figure 4). The highest Ti values are before 3.0 Ma. At 3.0 Ma, Ti counts decrease, and then there is a brief increase around 2.5 Ma, with three large Ti peaks around MIS 96-102. Outside of these periods, Ti remains relatively low (< 2000 counts). There is no clear glacial–interglacial variation in the Ti data.

4. Discussion

4.1 Climatic and oceanographic variability at ODP Site 1087 from 3.5 to 0.0 Ma

Overall, the Site 1087 records indicated a gradual transition from an upwelling-dominated record in the Pliocene and early Pleistocene to an Agulhas Leakage-dominated record in the mid- to late-Pleistocene (Figures 3; 4). During the late Pliocene (3.5–3.0 Ma), warmer SSTs, higher productivity, and a 6–7°C offset in the TEX₈₆⁻ and U₃₇^K’-derived temperatures suggest that more high nutrient Upwelling-sourced water reached Site 1087 (Petrick et al., 2015a). A period of lower

productivity and lower Ti counts marked the late Pliocene–early Pleistocene (3.0–2.0 Ma), with less terrestrial input and mostly stable SSTs. During this interval, there continued to be an offset between TEX_{86} - and U_{37}^{K} -derived temperatures, but this varied between 4 and 11°C, indicating variable upwelling intensity. The period between 1.5 and 0.6 Ma is characterised by an increase in productivity, cooler SSTs, and a reduction in the TEX_{86} - U_{37}^{K} temperature offset (Figure 2). Finally, the mid- to late-Pleistocene (0.6–0.0 Ma) is defined by warming SSTs, variable productivity with higher productivity during glacials, and lower terrestrial input (from Ti). These trends, coupled with the previously published data, indicate that, over the last 500 ka, there has been increased warm water input through the Agulhas Leakage during prominent interglacials, punctuated by glacial periods with high productivity (Petrick et al., 2015b). For a further analysis of the proxies used in making the reconstruction, please see the supplemental material.

It has been proposed that tectonic uplift along the Namibian coast since the Pliocene could have increased upwelling intensity and slowly shifted upwelling cells northward (Jung et al., 2014). Overall, the data from Site 1087 is broadly consistent with this hypothesis, but this time interval also includes several known global climate changes, which are hypothesised to have impacted subtropical upwelling systems. Here, we evaluate the links to other potential forcing mechanisms driven by Plio-Pleistocene climate evolution.

4.2. Late Pliocene (3.5–3.0 Ma)

The new XRF data from Site 1087 confirms that the oceanographic conditions during the late Pliocene (3.5–3.0 Ma) were very different from those observed in the modern environment at this location. The high Ti counts between 3.5 and 3.0 Ma are associated with high alkenone MAR (this study) and a significant offset between U_{37}^{K} and TEX_{86} -derived temperatures (Petrick et al., 2015). There is clear evidence of higher productivity, higher terrestrial input, and offsets in the different temperature proxies during the Pliocene relative to the modern, which suggests an influence of wind-driven upwelling at the site (Petrick et al., 2015a). The U_{37}^{K} SSTs at Site 1087 were much colder

than the Northern and Central Benguela Upwelling Systems (Fig. 5) (Rosell-Melé et al., 2014), but very similar to those at Site 1085 (Rommerskirchen et al., 2011). This large temperature difference between the northern/central and southern Benguela cells, over a relatively short area, is unusual in the Pliocene, when equator to pole gradients were often reduced (Fedorov et al., 2015). Rosell-Melé et al. (2014) suggested that the lower productivity in the northern and central cells during the Pliocene was related to overall warming in the Benguela Upwelling System, which allowed a shallow layer of warm water to restrict upwelling vigour, a phenomenon described as a “permanent Benguela Nino” (Rosell-Melé et al., 2014). Therefore, this suggests that higher productivity at Site 1087 could be related to the colder temperatures, at least during the Pliocene, although the U_{37}^K -TEX₈₆ gradient is more indicative of an increased upwelling influence in the southern Benguela region as the reason for enhanced productivity.

The XRF data indicates higher Pliocene Ti/Al values than in any other part of the record, suggesting higher terrestrial input (Figure 5). Today the site only lies at the edge of both dust and riverine input pathways. Thus, one can posit that the delivery pathways of terrestrial material to ODP Site 1087 must have been different during the Pliocene. We infer that this was likely related to the poleward shift in wind patterns in the Southern Hemisphere relative to today, which would have shifted dust delivery southward (Lawrence et al., 2013). Given that Ti/Al values are found to reflect dust input, this is the more likely assumption (Govin et al., 2012). However, It is also possible that increased riverine input from the African continent could have increased the amount of terrestrial input reaching the cape basin, as there is some evidence that Southwest Africa was wetter during the Pliocene (Maslin et al., 2012). We are currently unable to disentangle the respective influence of the two terrestrial inputs recorded here due to a lack of evidence, especially XRF records from other sites in the region, which would allow a better understating of how the terrestrial input pathways shifted during the Pliocene. However, what is clear is that, during the Pliocene, the Benguela Upwelling System was operating differently from the present day.

4.3 INHG and the early Pleistocene (3.0–1.5 Ma)

Equatorward movement of the major upwelling cells may have played an important role in the transition from the warm Pliocene to colder modern temperatures around the iNHG at 2.7 Ma (Fedorov et al., 2007). However, a closer look at data from Site 1087 suggests a more complex story than the standard narrative. Changes in the size and strength of permanent upwelling in the Southern Benguela Upwelling System occurred at the beginning and end of the iNHG, but not necessarily at 2.7 Ma. Between 3.0 and 2.4 Ma, when the majority of North Atlantic cooling associated with iNHG occurred, the proxies at Site 1087 are stable.

Between 3.0 and 1.5 Ma, there is conflicting evidence about the strength of the Southern Benguela Upwelling System at Site 1087. Colder SSTs continue to be recorded at Site 1087 relative to the Northern and Central Upwelling System (Figure 5), coupled with the continuing offset between $\text{TEX}_{86}^{\text{H}}$ and U_{37}^{K} -derived temperatures (Figure 2). Based on the recent work by Zhu et al. (2016), the best explanation for the continued offset between the two temperature records is that TEX_{86} is recording conditions in shallow waters (<100 m), most likely from the centre of the upwelling region along the coast. Therefore, from the temperature proxies, it appears that water from the coastal upwelling cells was reaching Site 1087 directly across the late Pliocene-early Pleistocene. However, around 3.0 Ma, there was a decrease in primary productivity as recorded in the alkenone and chlorin MAR combined with a corresponding decrease in Ti content, indicating a reduction in terrestrial input (Figures 4, 6). Thus, a clear difference emerges between the productivity data, which suggests reduced upwelling (lower productivity, less wind influence), and the temperature data, which suggests that upwelled waters continued to influence the site.

The differences between the productivity and temperature proxy records in upwelling systems can be explained by changes in the type of nutrients being delivered to the site, either through shifts in the local nutrient delivery paths or the nutrient content of the upwelled water (Dekens et al., 2007). The coupled decreases in Ti/Al and productivity around 3.0 Ma suggest a

connection between the loss of terrestrial input and productivity. One possibility is that a weakening or northward migration of the trade winds might have moved the major African dust plume northward (Figure 4; Etourneau et al., 2009; Martínez-García et al., 2011). It is thought that there were northward shifts in both the trade winds and westerlies during the Plio-Pleistocene transition (Etourneau et al., 2010). However, most of the shifts in the wind systems occur around 2.7 Ma, after the Site 1087 Ti/Al decreased (Etourneau et al., 2009; Lawrence et al., 2013). It is also possible that the Ti/Al decrease was related to changes in hydrology, as observed farther north at Site 1085, suggesting a drier west Africa (Maslin et al., 2012). The change in terrestrial input suggests that shifts occurred in the local wind fields and oceanic terrestrial delivery patterns around 3.0 Ma, which were likely partially related to changes in nutrient delivery to the site.

The low (non-diatom) productivity at Site 1087 occurred within the same time interval as the Matuyama Diatom Maximum (MDM; 3.0-2.0 Ma) in the rest of the Benguela Upwelling System (Leduc et al., 2014; Robinson and Meyers, 2002) (Figure 6). Changes in the type and amount of nutrients delivered to the upwelling zone could control the amount and type of primary productivity in the zone (Lawrence et al., 2006; März et al., 2013). The MDM, which started around 3.0 Ma in the northern and central cells, occurs at the same time as other biogenic silica increases in other upwelling cells all over the world (März et al., 2013). Increases in the Si content of the Antarctic Intermediate Water led to increases in the amount of biogenic silica production in global upwelling cells (März et al., 2013). In the Northern and Central Benguela Upwelling, this increase in diatom production occurred despite reduced upwelling strength (Leduc et al., 2014; Robinson and Meyers, 2002). We were unable to determine biogenic silica content at Site 1087, so we cannot consider directly the role of silicate supply on diatom production. However, the similarity of the timing between the start of the MDM and the decrease in upwelling means that it is likely that increases in biogenic silica in the Antarctic Intermediate Water were responsible for the decrease in non-silica productivity in the entire Benguela Upwelling System.

Between 2.4–2.0 Ma, U_{37}^K -derived SSTs decrease at Site 1087. There is a slight increase in alkenone MARs, but no increase in chlorin MARs and no change in terrestrial inputs (Figures 2, 3, and 6). During this interval, cooling of U_{37}^K -derived SSTs is also observed at Site 1084 (Figure 5), accompanied by evidence of upwelling intensification (Robinson and Meyers, 2002; Rosell-Melé et al., 2014), yet only alkenone MAR increases at Site 1087. Climate changes around 2.4 Ma have been previously linked to increases in the Walker Circulation (Brierley and Fedorov, 2010; Liu et al., 2008; Rosell-Melé et al., 2014). The increased Walker Circulation may have increased upwelling vigour, allowing nutrients from the coastal southern upwelling cells to be delivered to Site 1087. There is an increase in alkenone productivity at Site 1087 around 2.4 Ma. Therefore it is likely, given the similar timing of temperature and productivity changes in Sites 1087 and 1084, that the increasing strength of the Walker Circulation caused a northward expansion of upwelling in the Benguela Upwelling System (Etourneau et al., 2010).

Shifting global winds were not likely controlling the location, extent, temperature, or intensity of the Southern Benguela Upwelling System when other records show major equatorward shifts in upwelling at 2.7 Ma (Lawrence et al. 2013). Most of the system-wide upwelling changes seem to be driven by external shifts in the nutrients being delivered to the upwelling system from around 3.0 Ma. Instead, around 2.7 Ma, the Benguela Upwelling System is responding more to local changes in nutrient supply and upwelling temperatures. This is similar to the results seen in the Peruvian Margin, where changes in the SST within the upwelling zone occurred before 2.7 Ma (Dekens et al., 2007). Given the importance of coastal upwelling to nutrient cycling and CO_2 exchange, data emphasize the importance of understanding the impact of nutrient changes on coastal upwelling cells.

4.4 Mid- and Late Pleistocene (1.5–0.0 Ma)

Around 1.5 Ma, there is a change in the relationship between the Southern Benguela Upwelling System and the rest of the Benguela Upwelling System. SSTs decrease at Site 1087

between 1.5 and 0.9 Ma (across the MPT), accompanied by increases in Ca/Ti, with a later increase in chlorin MAR from 1.5 Ma and an increase in alkenone MAR from 1.1 Ma (Figures 2; 3). The U_{37}^K - SST cooling has a global component, as it was observed in all records from the SE Atlantic Ocean. However, it was 300-kyr earlier than most other basins, which show cooling starting around 1.2 Ma (Figure 4; Etourneau et al., 2010; Martinez-Garcia et al., 2010; McClymont et al., 2013; Rosell-Melé et al., 2014). From 1.5 Ma, the observed increase in chlorin MAR at Site 1087 is also accompanied by increases in the alkenone MAR in the northern and central cells (Rosell-Melé et al., 2014) (Figure 6). Therefore, it appears that at 1.5 Ma, both the Northern and Southern Benguela Upwelling System showed similar increase in productivity, which could indicate that there had been expansion of the Benguela Upwelling System to the north. In the southern Benguela Upwelling System, the large increases in Ca/Ti values coupled with increasing alkenone MARs indicate that the central upwelling cells were moving away from Site 1087, which was now influenced instead by the edge of the upwelling zone (Giraudeau et al., 1993; Giraudeau and Rogers, 1994). Increased coccolithophore deposition in the Benguela Upwelling System indicates a shift towards less turbulent conditions and a more marginal upwelling setting at Site 1087 (Giraudeau et al., 1993; Giraudeau and Rogers, 1994).

The data also shows less primary productivity during interglacials after 0.9 Ma (Petrack et al., 2015b) (Figure 2). From 0.9 Ma onward, there is a clear shift in the SST gradient between Sites 1087 and 1084, the latter of which inhabits the central upwelling cell (Figure 4), demonstrating a reduced connection between the two sites as upwelling at Site 1084 intensifies. We interpret this pattern as indicating an increasingly reduced influence of the Benguela Upwelling System at Site 1087, in turn reducing the productivity at the site during the glacial terminations and interglacials since 0.9 Ma, consistent with modern oceanography (Boebel et al., 2003). However, this occurs as the northern and central upwelling cells indicated increased productivity and cooling (Rosell-Melé et al., 2014), suggesting that the modern day extent of upwelling started around 0.6 Ma (Rosell-Melé et al., 2014). This is confirmed by coeval increases in the Ca/Ti ratio at Site 1087 across the entire mid- to late-Pleistocene (Figure 3), which is supportive of a more marginal upwelling setting. Despite the overall

trend of decreasing upwelling influence at ODP Site 1087, during the earlier ‘glacial’ modes of the upwelling there are often short increases in upwelling strength, as determined by increases in chlorin MARs (Petrick et al. 2015a).

After 0.9 Ma, the TEX_{86} and U_{37}^{K} -derived temperatures at Site 1087 converged, and SSTs warm by 2° C between 0.6 and 0.0 Ma. This increase was superimposed upon large amplitude variations in all the proxy records (Figures 3; 4), which occurred at the same time as the onset of the quasi-100-kyr glacial-interglacial cycles that mark the Early Mid-Pleistocene Transition (EMPT) (Maslin and Brierley, 2015). After the EMPT, the pattern of glacials and interglacials changes to a tripartite mode composed of an interglacial, a glacial and a full glacial (Maslin and Brierley, 2015). At ODP Site 1087 productivity decreases, and the abundance of the Agulhas Leakage indicator foraminifera, *G. menardii*, increases during the ‘full glacial’ portion of the deglaciation over the last 1.2 Ma (Caley et al., 2014, 2012). This is around the same time that the relationship between the various SST proxies changes and average temperatures start increasing. Furthermore, previous work has showed that increases in temperature at ODP 1087 had the exact same timings as temperature increases in the leakage zone proper (Caley et al., 2014, 2012; Petrick et al., 2015b). Increased Agulhas Leakage therefore might be linked to the start of the quasi-100-kyr post-EMPT cycles (Caley et al., 2014, 2012; Peeters et al., 2004). However, the changes in temperature could also be linked to the previously mentioned reduction in Benguela Upwelling around ODP 1087. Furthermore, studies show that changes in temperature and salt leakage do not necessarily relate to changes in the amount of Agulhas Leakage (Simon et al., 2015). Despite this, there is a major change in the effect of the Agulhas Leakage on the site after the EMPT. Therefore, even if there was not any change in the location or strength of the Agulhas Leakage, it is still clear that there was a major reorganization of the SE Atlantic that allowed it to have a more direct impact on ODP site 1087. Future studies are needed to better understand the changes in the Agulhas Leakage over the last 3.5 Ma.

5. Conclusions

New geochemical data from ODP Site 1087 reveal a complex timing of shifts in the intensity of the Southern Benguela Upwelling System and the initiation of increased Agulhas Leakage over the Pliocene and Pleistocene. First, records indicate that the Southern Benguela Upwelling System was also influenced by the changes in nutrients and by warmer SSTs between 3.0 and 2.0 Ma. There is no evidence for a northward movement of the focus or extent of upwelling around 2.7 Ma, suggesting that changes in the wind fields had limited/no impact over the extent and strength of the upwelling during the iNHG. Finally, northward movement of the Benguela Upwelling System occurred around 0.9 Ma, such that Site 1087 becomes dominated by the effects of Agulhas Leakage by 0.6 Ma. This observation suggests that oceanographic changes during the MPT established the modern extent of the Benguela Upwelling System and Agulhas Leakage. Considered together, these factors demonstrate that the development of the modern extent of upwelling, at least in the SE Atlantic, was complex and different from the linear northward progression that has been seen in other open ocean upwelling cells. This emphasises the importance of reconstructing information from multiple sites within an upwelling system to better understand the complete picture of upwelling development.

Acknowledgements.

The authors would like to thank Newcastle University and the Department of Geography for funding this research through a School studentship. I would also like to thank the University college of London and University of Bristol for providing resources as well. Additional funding came from Durham University and the Max Planck Society. ELM acknowledges the support of a Philip Leverhulme Prize. I would also like to thank IODP for providing the samples to work on and the MARUM in Bremen for use of the scanning XRF. I would like to thank Tomas Westerhold, Alfredo Martinez-Garcia, Gerald Auer and Jessie Farmer for their input on the data. I would also like to thank James Petrick for copy editing the article. The data will be available in PANGEA on

final publication. I would also like to thank the editor Martin Frank and three anonymous reviewers for their helpful comments.

Citations

- Barreiro, M., Philander, G., Pacanowski, R., Fedorov, A., 2005. Simulations of warm tropical conditions with application to middle Pliocene atmospheres. *Clim. Dyn.* 26, 349–365. doi:10.1007/s00382-005-0086-4
- Beal, L.M., De Ruijter, W.P.M., Biastoch, A., Zahn, R., 136, S.W.G., Cronin, M., Hermes, J., Lutjeharms, J., Quartly, G., Tozuka, T., Baker-Yeboah, S., Bornman, T., Cipollini, P., Dijkstra, H., Hall, I., Park, W., Peeters, F., Penven, P., Ridderinkhof, H., Zinke, J., 2011. On the role of the Agulhas system in ocean circulation and climate. *Nature* 472, 429–436. doi:10.1038/nature09983
- Biastoch, A., Böning, C.W., Lutjeharms, J.R.E., 2008. Agulhas leakage dynamics affects decadal variability in Atlantic overturning circulation. *Nature* 456, 489–492. doi:10.1038/nature07426
- Bluck, B.J., Ward, J.D., Cartwright, J., Swart, R., 2007. The Orange River, southern Africa: an extreme example of a wave-dominated sediment dispersal system in the South Atlantic Ocean. *J. Geol. Soc. London.* 164, 341–351. doi:10.1144/0016-76492005-189
- Boebel, O., Lutjeharms, J., Schmid, C., Zenk, W., Rossby, T., Barron, C., 2003. The Cape Cauldron: a regime of turbulent inter-ocean exchange. *Deep. Res. Part II-Topical Stud. Oceanogr.* 50, 57–86.
- Brierley, C.M., Fedorov, A. V., 2010. Relative importance of meridional and zonal sea surface temperature gradients for the onset of the ice ages and Pliocene-Pleistocene climate evolution. *Paleoceanography* 25, PA2214. doi:10.1029/2009PA001809
- Caley, T., Giraudeau, J., Malaize, B., Rossignol, L., Pierre, C., 2012. Agulhas leakage as a key process in the modes of Quaternary climate changes. *Proc. Natl. Acad. Sci.* 109, 6835–6839. doi:10.1073/pnas.1115545109
- Caley, T., Peeters, F.J.C., Biastoch, A., Rossignol, L., Sebille, E. Van, 2014. *Geophysical Research Letters* 1238–1246. doi:10.1002/2014GL059278. Received
- Chalk, T.B., Hain, M.P., Foster, G.L., Rohling, E.J., Sexton, P.F., Badger, M.P.S., Cherry, S.G., Hasenfratz, A.P., Haug, G.H., Jaccard, S.L., Martínez-García, A., Pälike, H., Pancost, R.D., Wilson, P.A., 2017. Causes of ice age intensification across the Mid-Pleistocene Transition. *Proc. Natl. Acad. Sci.* 114, 201702143. doi:10.1073/pnas.1702143114
- Christensen, B.A., Giraudeau, J., 2002. Neogene and Quaternary evolution of the Benguela upwelling system - Foreword. *Mar. Geol.* 180, 1–2.
- Compton, J., Herbert, C., Schneider, R., 2009. Organic-rich mud on the western margin of southern Africa: Nutrient source to the Southern Ocean? *Glob. Biogeochem. Cycles* 23, GB4030. doi:10.1029/2008gb003427
- Compton, J.S., Maake, L., 2007. Source of the suspended load of the upper Orange River, South Africa. *South African J. Geol.* 110, 339–348. doi:10.2113/gssajg.110.2-3.339
- Dekens, P.S., Ravelo, A.C., McCarthy, M.D., 2007. Warm upwelling regions in the Pliocene warm period. *Paleoceanography* 22, PA3211. doi:10.1029/2006pa001394
- Diester-Haass, L., 1988. Sea level changes, carbonate dissolution and history of the Benguela Current in the Oligocene-Miocene off Southwest Africa (DSDP Site 362, Leg 40). *Mar. Geol.* 79, 213–242. doi:10.1016/0025-3227(88)90040-0
- Dyez, K.A., Zahn, R., Hall, I.R., 2014. Multicentennial Agulhas leakage variability and links to North

516 Atlantic climate during the past 80,000 years. *Paleoceanography* 29, 1238–1248.
517 doi:10.1002/2014PA002698

518 Etourneau, J., Martinez, P., Blanz, T., Schneider, R., 2009. Pliocene-Pleistocene variability of
519 upwelling activity, productivity, and nutrient cycling in the Benguela region. *Geology* 37, 871–
520 874. doi:10.1130/G25733A.1

521 Etourneau, J., Schneider, R., Blanz, T., Martinez, P., 2010. Intensification of the Walker and Hadley
522 atmospheric circulations during the Pliocene-Pleistocene climate transition. *Earth Planet. Sci.*
523 *Lett.* 297, 103–110. doi:10.1016/j.epsl.2010.06.010

524 Fedorov, A., Barreiro, M., Boccaletti, G., Pacanowski, R., Philander, S.G., 2007. The Freshening of
525 Surface Waters in High Latitudes: Effects on the Thermohaline and Wind-Driven Circulations. *J.*
526 *Phys. Oceanogr.* 37, 896–907. doi:10.1175/jpo3033.1

527 Fedorov, A. V., Burls, N.J., Lawrence, K.T., Peterson, L.C., 2015. Tightly linked zonal and meridional
528 sea surface temperature gradients over the past five million years. *Nat. Geosci.* 8, 975–980.
529 doi:10.1038/ngeo2577

530 Giraudeau, J., Monteiro, P.M.S., Nikodemus, K., 1993. Distribution and malformation of living
531 coccolithophores in the northern Benguela upwelling system off Namibia. *Mar. Micropaleontol.*
532 22, 93–110. doi:10.1016/0377-8398(93)90005-I

533 Giraudeau, J., Rogers, J., 1994. Phytoplankton Biomass and Sea-Surface Temperature Estimates from
534 Sea-Bed Distribution of Nannofossils and Planktonic Foraminifera in the Benguela Upwelling
535 System. *Micropaleontology* 40, 275. doi:10.2307/1485822

536 Gordon, A.L., Haxby, W.F., 1990. Agulhas Eddies Invade the South Atlantic: Evidence From Geosat
537 Altimeter and Shipboard Conductivity-Temperature-Depth Survey. *J. Geophys. Res.* 95, 3117–
538 3125. doi:10.1029/JC095iC03p03117

539 Gordon, A.L., Lutjeharms, J.R.E., Gründlingh, M.L., 1987. Stratification and circulation at the Agulhas
540 Retroflexion. *Deep Sea Res. Part A. Oceanogr. Res. Pap.* 34, 565–599.

541 Govin, A., Holzwarth, U., Heslop, D., Ford Keeling, L., Zabel, M., Mulitza, S., Collins, J.A., Chiessi, C.M.,
542 2012. Distribution of major elements in Atlantic surface sediments (36°N-49°S): Imprint of
543 terrigenous input and continental weathering. *Geochemistry, Geophys. Geosystems* 13, n/a-
544 n/a. doi:10.1029/2011GC003785

545 Hall, C., Lutjeharms, J.R.E., 2011. Cyclonic eddies identified in the Cape Basin of the South Atlantic
546 Ocean. *J. Mar. Syst.* 85, 1–10.

547 Harris, P.G., Zhao, M., Rosell-Mele, A., Tiedemann, R., Sarnthein, M., Maxwell, J.R., 1996. Chlorin
548 accumulation rate as a proxy for Quaternary marine primary productivity. *Nature* 383, 63–65.

549 Haug, G.H., Ganopolski, A., Sigman, D.M., Rosell-Mele, A., Swann, G.E.A., Tiedemann, R., Jaccard,
550 S.L., Bollmann, J., Maslin, M.A., Leng, M.J., Eglinton, G., 2005. North Pacific seasonality and the
551 glaciation of North America 2.7 million years ago. *Nature* 433, 821–825.
552 doi:10.1038/nature03332

553 Jung, G., Prange, M., Schulz, M., 2014. Uplift of Africa as a potential cause for Neogene
554 intensification of the Benguela upwelling system. *Nat. Geosci. advance on*, 741–747.
555 doi:10.1038/ngeo2249

556 Kienast, S.S., Winckler, G., Lippold, J., Albani, S., Mahowald, N.M., 2016. Tracing dust input to the
557 global ocean using thorium isotopes in marine sediments: ThoroMap. *Global Biogeochem.*
558 *Cycles* 30, 1526–1541. doi:10.1002/2016GB005408

559 Knorr, G., Lohmann, G., 2003. Southern Ocean origin for the resumption of Atlantic thermohaline
560 circulation during deglaciation. *Nature* 424, 532–536. doi:10.1038/nature01855

561 Kornilova, O., Rosell-Mele, A., 2003. Application of microwave-assisted extraction to the analysis of

562 biomarker climate proxies in marine sediments. *Org. Geochem.* 34, 1517–1523.
563 doi:10.1016/s0146-6380(03)00155-4

564 Lawrence, K.T., Liu, Z., Herbert, T.D., 2006. Evolution of the eastern tropical Pacific through Plio-
565 Pleistocene glaciation. *Science* 312, 79–83. doi:10.1126/science.1120395

566 Lawrence, K.T., Sigman, D.M., Herbert, T.D., Riihimäki, C.A., Bolton, C.T., Martinez-Garcia, A., Rosell-
567 Mele, A., Haug, G.H., 2013. Time-transgressive North Atlantic productivity changes upon
568 Northern Hemisphere glaciation. *Paleoceanography* 28, 740–751. doi:10.1002/2013PA002546

569 Leduc, G., Garbe-Schönberg, D., Regenberg, M., Contoux, C., Etourneau, J., Schneider, R., 2014. The
570 late Pliocene Benguela upwelling status revisited by means of multiple temperature proxies.
571 *Geochemistry, Geophys. Geosystems* 15, 475–491. doi:10.1002/2013GC004940

572 Liu, Z.H., Altabet, M.A., Herbert, T.D., 2008. Plio-Pleistocene denitrification in the eastern tropical
573 North Pacific: Intensification at 2.1 Ma. *Geochemistry Geophys. Geosystems* 9, 14.
574 doi:10.1029/2008GC002044

575 Mahowald, N., Albani, S., Kok, J.F., Engelstaeder, S., Scanza, R., Ward, D.S., Flanner, M.G., 2014. The
576 size distribution of desert dust aerosols and its impact on the Earth system. *Aeolian Res.* 15,
577 53–71. doi:10.1016/j.AEOLIA.2013.09.002

578 Marino, G., Zahn, R., Ziegler, M., Purcell, C., Knorr, G., Hall, I.R., Ziveri, P., Elderfield, H., 2013.
579 Agulhas salt-leakage oscillations during abrupt climate changes of the Late Pleistocene.
580 *Paleoceanography* 28, 599–606. doi:10.1002/palo.20038

581 Marlow, J.R., Lange, C.B., Wefer, G., Rosell-Mele, A., 2000. Upwelling intensification as part of the
582 Pliocene-Pleistocene climate transition. *Science* (80-.). 290, 2288–+.

583 Martínez-Garcia, A., Rosell-Melé, A., Jaccard, S.L., Geibert, W., Sigman, D.M., Haug, G.H., Martinez-
584 Garcia, A., Rosell-Mele, A., Jaccard, S.L., Geibert, W., Sigman, D.M., Haug, G.H., 2011. Southern
585 Ocean dust–climate coupling over the past four million years. *Nature* 476, 312–315.
586 doi:10.1038/nature10310

587 Martinez-Garcia, A., Rosell-Mele, A., McClymont, E.L., Gersonde, R., Haug, G.H., 2010. Subpolar Link
588 to the Emergence of the Modern Equatorial Pacific Cold Tongue. *Science* (80-.). 328, 1550–
589 1553. doi:10.1126/science.1184480

590 März, C., Schnetger, B., Brumsack, H.-J., 2013. Nutrient leakage from the North Pacific to the Bering
591 Sea (IODP Site U1341) following the onset of Northern Hemispheric Glaciation?
592 *Paleoceanography* 28, 68–78. doi:10.1002/palo.20011

593 Maslin, M.A., Brierley, C.M., 2015. The role of orbital forcing in the Early Middle Pleistocene
594 Transition. *Quat. Int.* 389, 47–55. doi:10.1016/j.quaint.2015.01.047

595 Maslin, M.A., Pancost, R.D., Wilson, K.E., Lewis, J., Trauth, M.H., 2012. Three and half million year
596 history of moisture availability of South West Africa: Evidence from ODP site 1085 biomarker
597 records. *Palaeogeogr. Palaeoclimatol. Palaeoecol.* 317–318, 41–47.
598 doi:10.1016/j.palaeo.2011.12.009

599 McClymont, E.L., Rosell-Melé, A., Giraudeau, J., Pierre, C., Lloyd, J.M., 2005. Alkenone and coccolith
600 records of the mid-Pleistocene in the south-east Atlantic: Implications for the U37K' index and
601 South African climate. *Quat. Sci. Rev.* 24, 1559–1572. doi:10.1016/j.quascirev.2004.06.024

602 McClymont, E.L., Sosdian, S.M., Rosell-Melé, A., Rosenthal, Y., 2013. Pleistocene sea-surface
603 temperature evolution: Early cooling, delayed glacial intensification, and implications for the
604 mid-Pleistocene climate transition. *Earth-Science Rev.* 123, 173–193.
605 doi:10.1016/j.earscirev.2013.04.006

606 Müller, P.J., Kirst, G., Ruhland, G., von Storch, I., Rosell-Mele, A., 1998. Calibration of the alkenone
607 paleotemperature index U-37(K') based on core-tops from the eastern South Atlantic and the

- global ocean (60 degrees N-60 degrees S). *Geochim. Cosmochim. Acta* 62, 1757–1772.
- Peeters, F.J.C., Acheson, R., Brummer, G.-J.A., de Ruijter, W.P.M., Schneider, R.R., Ganssen, G.M., Ufkes, E., Kroon, D., 2004. Vigorous exchange between the Indian and Atlantic oceans at the end of the past five glacial periods. *Nature* 430, 661–665.
- Petrack, B., McClymont, E.L., Felder, S., Rueda, G., Leng, M.J.M.J., Rosell-Melé, A., 2015. Late Pliocene upwelling in the Southern Benguela region. *Palaeogeogr. Palaeoclimatol. Palaeoecol.* 429, 62–71. doi:10.1016/j.palaeo.2015.03.042
- Petrack, B.F., McClymont, E.L., Marret, F., Van Der Meer, M.T.J., 2015. Changing surface water conditions for the last 500 ka in the Southeast Atlantic: Implications for variable influences of Agulhas leakage and Benguela upwelling. *Paleoceanography* In revisio, 1153–1167. doi:10.1002/2015PA002787
- Prahl, F.G., Wakeham, S.G., 1987. Calibration of unsaturation patterns in long-chain ketone compositions for palaeotemperature assessment. *Nature* 330, 367–369.
- Robinson, R.S., Meyers, P.A., 2002. Biogeochemical changes within the Benguela Current upwelling system during the Matuyama Diatom Maximum: Nitrogen isotope evidence from Ocean Drilling Program Sites 1082 and 1084. *Paleoceanography* 17, 16-1-16–10. doi:10.1029/2001pa000659
- Rommerskirchen, F., Condon, T., Mollenhauer, G., Dupont, L., Schefuss, E., 2011. Miocene to Pliocene development of surface and subsurface temperatures in the Benguela Current system. *Paleoceanography* 26, 15. doi:10.1029/2010pa002074
- Rosell-Melé, A., Martínez-García, A., McClymont, E.L., 2014. Persistent warmth across the Benguela upwelling system during the Pliocene epoch. *Earth Planet. Sci. Lett.* 386, 10–20. doi:10.1016/j.epsl.2013.10.041
- Schouten, S., Hopmans, E.C., Schefuss, E., Damste, J.S.S., 2002. Distributional variations in marine crenarchaeotal membrane lipids: a new tool for reconstructing ancient sea water temperatures? (vol 204, pg 265, 2002). *Earth Planet. Sci. Lett.* 204, 265–274.
- Scussolini, P., Marino, G., Brummer, G.-J.A.G.-J.A., Peeters, F.J.C.C., 2015. Saline Indian Ocean waters invaded the South Atlantic thermocline during glacial termination II. *Geology* 43, 139–142. doi:10.1130/G36238.1
- Shipboard Scientific Party, 1998. Site 1087, in: Wefer Berger, W.H., Richter, C., et al., G. (Ed.), *Proc. ODP, Init. Repts. Ocean Drilling Program, College Station, TX*, pp. 457–484.
- Simon, M.H., Gong, X., Hall, I.R., Ziegler, M., Barker, S., Knorr, G., van der Meer, M.T.J., Kasper, S., Schouten, S., 2015. Salt exchange in the Indian-Atlantic Ocean Gateway since the Last Glacial Maximum: A compensating effect between Agulhas Current changes and salinity variations? *Paleoceanography* 30, 1318–1327. doi:10.1002/2015PA002842
- West, S., Jansen, J.H.F., Stuut, J.B., 2004. Surface water conditions in the Northern Benguela Region (SE Atlantic) during the last 450 ky reconstructed from assemblages of planktonic foraminifera. *Mar. Micropaleontol.* 51, 321–344. doi:http://dx.doi.org/10.1016/j.marmicro.2004.01.004
- Zachos, J.C., Kroon, D., Blum, P., 2004. Shipboard Scientific Party 2 208.

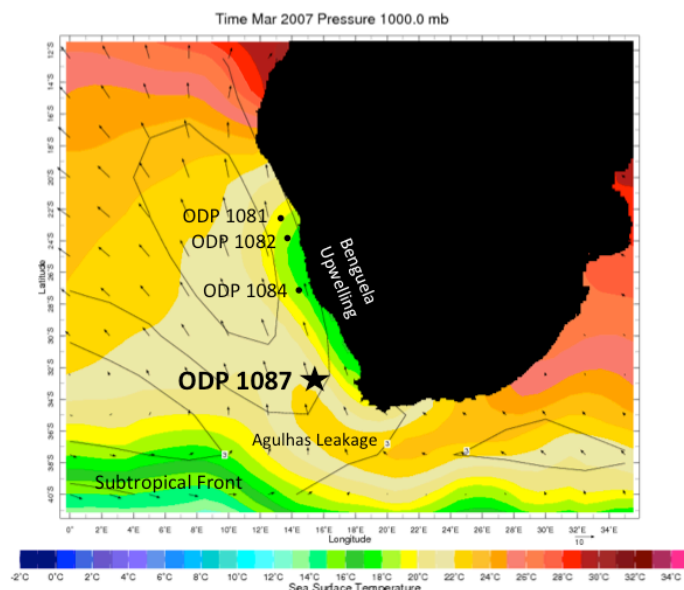


Figure 1: SE Atlantic map and relevant ODP drilling sites on an average SST record based on observational data for March 2007 from <http://iridl.ldeo.columbia.edu/>. Also shown are wind direction and pressure contours. The location of complementary records from this region referenced in the paper and the location of major oceanic systems in their modern day positions are shown.

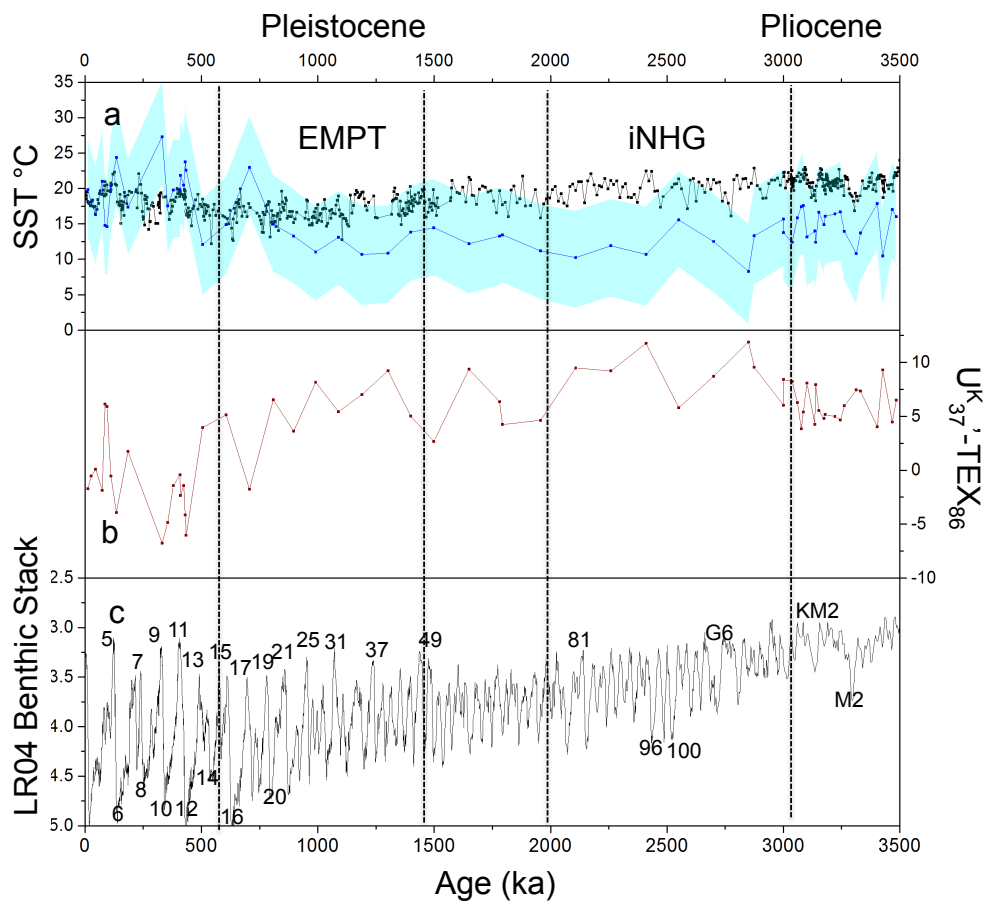


Figure 2: Temperature proxies for ODP Site 1087: a) sea surface temperature estimates derived from U_{37}^K (black line) and TEX_{86} BAYSPAR (blue line with dots) with analytical + calibration error envelope (blue envelope); b) Difference between U_{37}^K and TEX_{86} BAYSPAR derived SST estimates; c) LR04 benthic oxygen isotope stack (Lisiecki and Raymo, 2005) with selected MIS shown. Also major transitions in the ODP site 1087 record are shown with dashed lines and the timings of the iNGH and EMPT are labelled.

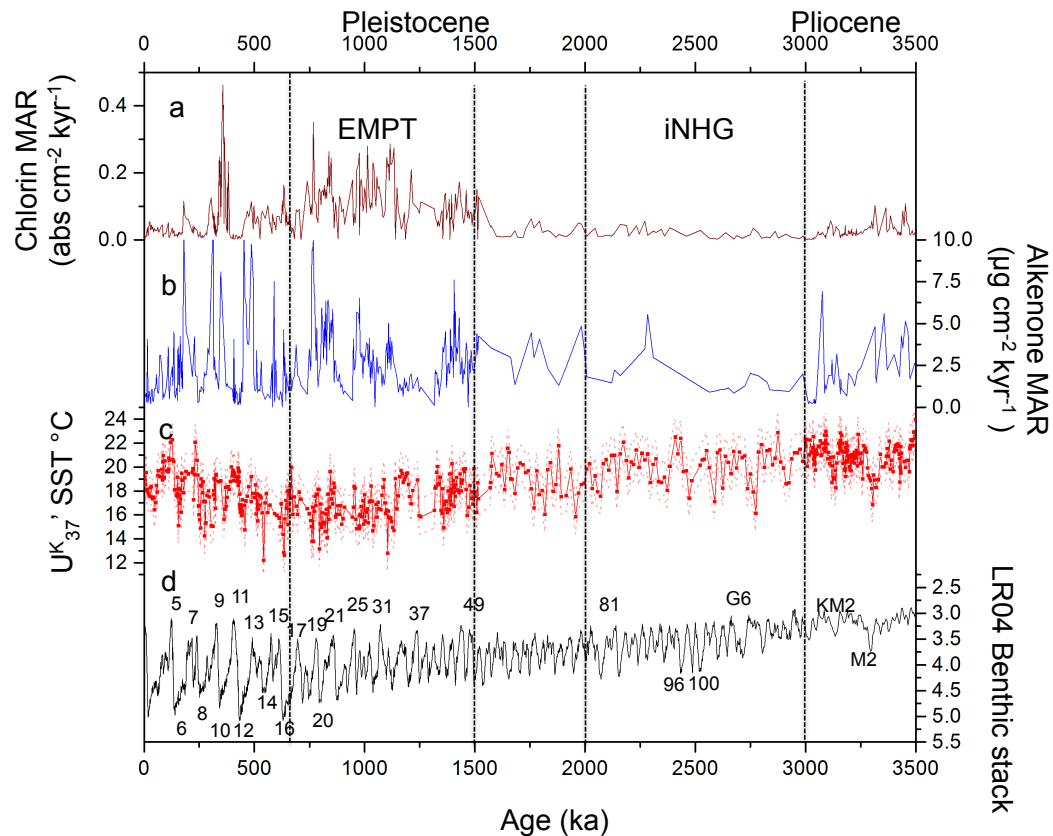


Figure 3: Productivity and temperature trends from ODP Site 1087: a) chlorin MARs; b) alkenone MARs; c) U_{37}^K -derived SSTs with error envelope; d) LR04 benthic oxygen isotope stack (Lisiecki and Raymo, 2005) with selected MIS shown. The vertical dashed lines indicate the major transitions observed in the data in terms of temperature and productivity. Also major transitions in the ODP site 1087 record are shown with dashed lines and the timings of the iNGH and EMPT are labelled.

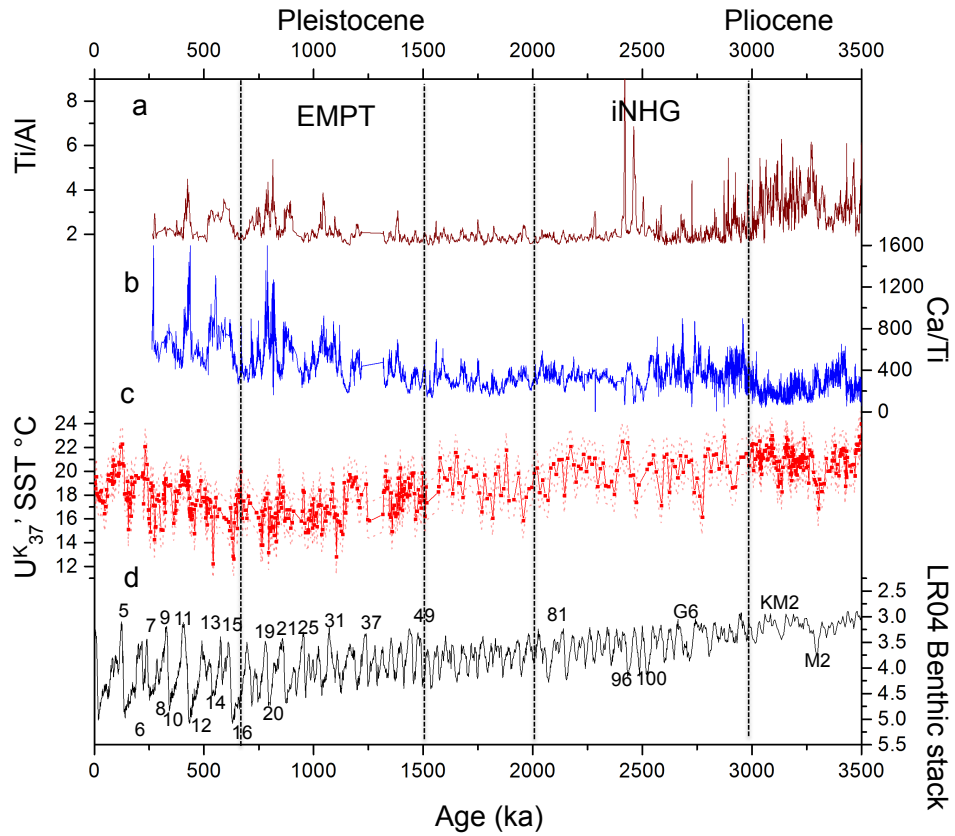


Figure 4: XRF data and temperature from ODP Site 1087: a) Ti/Al generated by scanning XRF; b) Ca/Ti data; c) U^K_{37} -derived SSTs, with error envelope including analytical plus calibration error; d) LR04 benthic oxygen isotope stack (Lisiecki and Raymo, 2005) with selected MIS shown. Major transitions in the ODP site 1087 record are shown with dashed lines and the timings of the iNHG and EMPT are labelled.

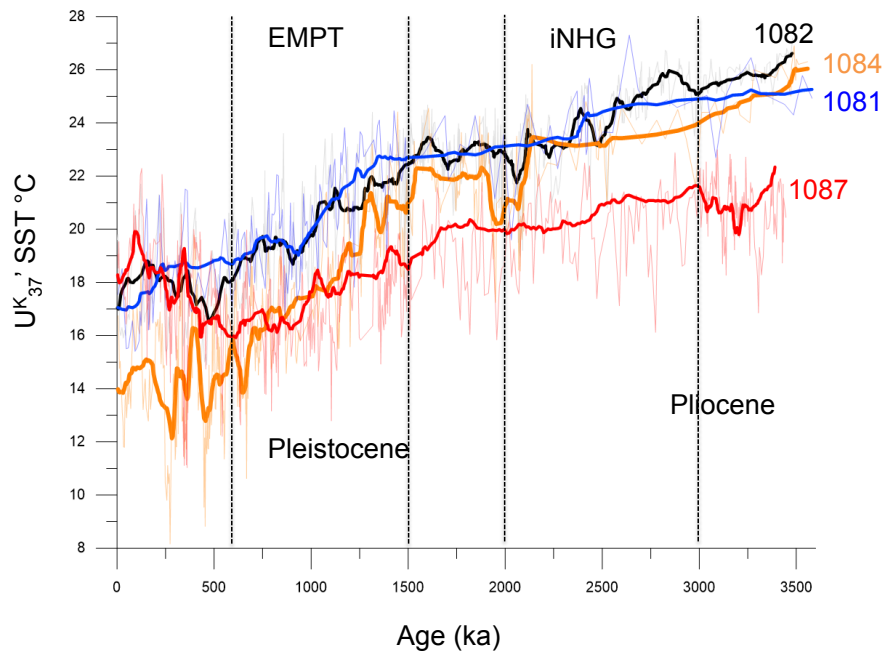


Figure 5: Regional SST trends. Comparing the ODP Site 1087 U_{37}^K -derived SST record (red) to the three other Benguela Upwelling SST records: ODP Sites 1082 (black), Site 1084 (orange), and Site 1081 (blue). The dark lines for each record represent 30 point running averages. Also, major transitions in the ODP site 1087 record are shown with dashed lines and the timings of the iNHG and EMPT are labelled.

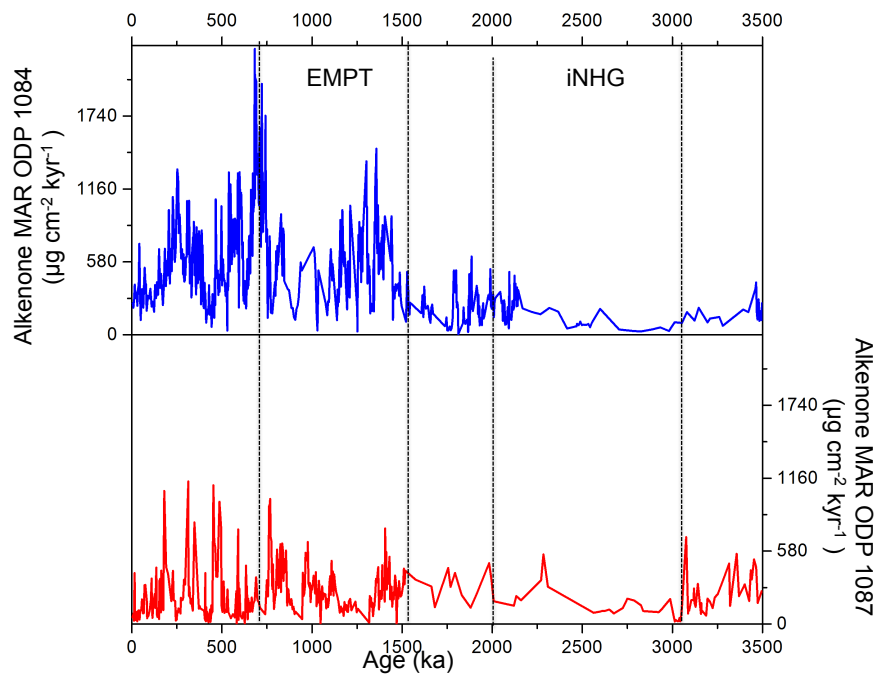


Figure 6: Alkenone MAR records from the Benguela Upwelling system over the Plio-Pleistocene: southern cells, ODP Site 1087 (red); central cells, ODP Site 1084 (blue). Both graphs are on the same scale so that a straight comparison of the two records can be done. Also, major transitions in the ODP site 1087 record are shown with dashed lines and the timings of the iNHG and EMPT are labelled.

689

690